Circulation Journal
Official Journal of the Japanese Circulation Society
http://www.j-circ.or.jp

ORIGINAL ARTICLE
Arrhythmia/Electrophysiology

Transmural Dispersion of Repolarization Determines Scroll Wave Behavior During Ventricular Tachyarrhythmias

– A Simulation Study –

Ryo Haraguchi, PhD; Takashi Ashihara, MD, PhD; Tsunetoyo Namba, MD, PhD; Kunichika Tsumoto, PhD; Shingo Murakami, PhD; Yoshihisa Kurachi, MD, PhD; Takanori Ikeda, MD, PhD; Kazuo Nakazawa, PhD

Background: Ventricular tachyarrhythmia is the leading cause of sudden cardiac death, and scroll wave re-entry is known to underlie this condition. Class III antiarrhythmic drugs are commonly used worldwide to treat ventricular tachyarrhythmias; however, these drugs have a proarrhythmic adverse effect and can cause Torsade de Pointes or ventricular fibrillation. Transmural dispersion of repolarization (TDR) has been suggested to be a strong indicator of ventricular tachyarrhythmia induction. However, the role of TDR during sustained scroll wave re-entry is poorly understood. The purpose of the present study was to investigate how TDR affects scroll wave behavior and to provide a novel analysis of the mechanisms that sustain tachyarrhythmias, using computer simulations.

Methods and Results: Computer simulations were carried out to quantify the TDR and QT interval under a variety of I_{Ks} and I_{Kr} during transmural conduction. Simulated scroll wave re-entries were done under a variety of I_{Ks} and I_{Kr} in a ventricular wall slab model, and the scroll wave behavior and the filament dynamics (3-dimensional organizing center) were analyzed. A slight increase in TDR, but not in the QT interval, reflected antiarrhythmic properties resulting from the restraint of scroll wave breakup, whereas a marked increase in TDR was proarrhythmic, as a result of scroll wave breakup.

Conclusions: The TDR determines the sustainment of ventricular tachyarrhythmias, through control of the scroll wave filament dynamics. (*Circ J* 2011; **75:** 80–88)

Key Words: Filament; Scroll wave re-entry; Simulation; Transmural dispersion of repolarization; Ventricular tachyarrhythmias/fibrillation

Class III antiarrhythmic drugs primarily block potassium channels, thereby prolonging both the cardiac action potential duration (APD) and QT interval. Prolongation of the APD with no change in conduction velocity terminates re-entrant tachyarrhythmias. Conversely, class III antiarrhythmic drugs have a proarrhythmic adverse effect, because prolonged APD causes ventricular tachyarrhythmias, particularly Torsade de Pointes (TdP)[1] and ventricular fibrillation (VF).

Editorial p 49

The mechanisms underlying drug-induced cardiac arrhythmias are not well understood, but it is widely accepted that the marked prolongation in APD and QT interval induced by I_{Kr}-blockade, especially during bradycardia, forms the substrate for the TdP and/or VF. Optical mapping studies have demonstrated that transmural dispersion of repolarization (TDR) plays a critical role in the initiation of TdP/VF in canine models of type-2 long QT syndrome (LQTS) and heart failure.[2,3] Furthermore, recent experimental studies using intracellular floating microelectrodes in arterially perfused canine left ventricular wedge preparations suggested that TDR was a strong indicator of TdP/VF induction.[4–6] Shimizu and Antzelevitch suggested that antiarrhythmic drugs that prolong the QT interval do not always have a proarrhythmic

Received January 25, 2010; revised manuscript received August 12, 2010; accepted August 20, 2010; released online November 16, 2010 Time for primary review: 45 days

National Cerebral and Cardiovascular Center Research Institute, Suita (R.H., K.N.); Department of Cardiovascular and Respiratory Medicine, Heart Rhythm Center, Shiga University of Medical Science, Otsu (T.A.); Faculty of Healthcare Sciences, Himeji Dokkyo University, Himeji (T.N.); The Center for Advanced Medical Engineering and Informatics, Osaka University, Suita (K.T.); Department of Pharmacology, Graduate School of Medicine, Osaka University, Suita (S.M., Y.K.); and Second Department of Internal Medicine, Kyorin University School of Medicine, Mitaka (T.I.), Japan

Mailing address: Ryo Haraguchi, PhD, National Cerebral and Cardiovascular Center Research Institute, 5-7-1 Fujishiro-dai, Suita 565-8565, Japan. E-mail: haraguch@ri.ncvc.go.jp

ISSN-1346-9843 doi:10.1253/circj.CJ-10-0071

All rights are reserved to the Japanese Circulation Society. For permissions, please e-mail: cj@j-circ.or.jp

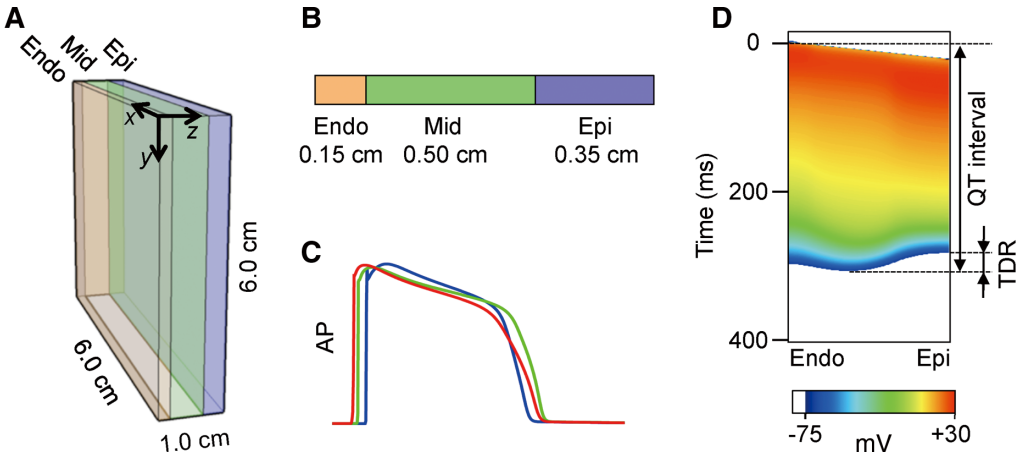

Figure 1. (**A**) 3-dimensional (D) ventricular wall slab model and (**B**) transmural 1-D model. Endo, Mid, and Epi indicate endocardial, mid-myocardial, and epicardial layers, respectively. (**C**) Action potential (AP) waveforms at Endo (red), Mid (green), and Epi (blue). (**D**) Space-time plot of membrane potentials. These waveforms and membrane potentials were measured after 31 constant pacing stimuli of 5-ms duration and 20-μA strength were applied to the endocardial units at a cycle of length of 1,000 ms. TDR, transmural dispersion of repolarization.

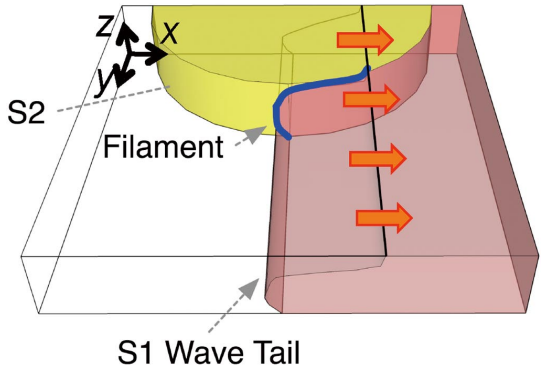

Figure 2. An S1-S2 method for generating a scroll wave in the ventricular wall slab model. S1 indicates the first planar wave that propagates from left to right along the ***x***-axis. The pink-coded region represents the excitation wave (both the depolarized and repolarizing region), whereas the colorless region represents the excitable area (repolarized region following the S1 planar wave). S2 is a premature stimulus (yellow region) in globular shape. The scroll wave starts to rotate around a filament (blue line) in a transmural location.

Table. Maximum Conductances of I_{Ks} in the Model

	Original I_{Ks} model (mS/μF)	Reduced I_{Ks} model (mS/μF)
Endo	$0.08240 \cdot A$	$0.01648 \cdot A$
Mid	$0.04118 \cdot A$	$0.008236 \cdot A$
Epi	$0.08240 \cdot A$	$0.01648 \cdot A$

$$A = 1 + \frac{0.6}{1 + \left(\frac{0.000038}{[Ca^{2+}]_i}\right)^{1.4}}$$

Endo, endocardial; Mid, mid-myocardial; Epi, epicardial; $[Ca^{2+}]_i$, intracellular concentration of Ca^{2+}.

adverse effect, but the reduction of TDR might eliminate the substrate for re-entry induction.[4] Diego et al demonstrated that the risk for TdP induction was related to the increase in TDR, rather than in the QT interval.[7]

Scroll wave re-entry is the active source of excitation that sustains ventricular tachyarrhythmias. However, the role of TDR during scroll wave re-entry is not well understood. To investigate how TDR affects the behavior of scroll wave re-entry, we conducted computer simulations of scroll wave re-entries under various conditions of TDR in a 3-dimensional (D) ventricular wall slab model. We have been conducting many computer simulations of scroll wave re-entries in an anatomically-detailed 3-D ventricular model.[8,9] Through this research, we revealed that anatomical features play an important role when considering the behavior of scroll wave re-entries. In this research, therefore, we removed anatomical features that were expected to lead to complications and over-analysis as much as possible. We focused on the dynamics of the filament, the scroll wave-organizing center, to simplify and quantify the complex spatiotemporal activity during scroll wave re-entry.[10]

Methods

The membrane kinetics in the simulated myocardium were produced by Luo-Rudy dynamic model equations[11] with modification of the L-type calcium channel formulation and introduction of 4 representative types of I_{Kr}-blockade: dofetilide, quinidine, vesnarinone, and nifekalant.[12,13] Dofetilide-induced blockade is voltage- and time-independent, quinidine-induced blockade is fast-voltage- and time-dependent, and vesnarinone-induced blockade is slow-voltage- and time-dependent. Nifekalant-induced blockade was simulated using a steady-state activation curve of I_{Kr} kinetics shifted positively.[14] The numerical approach for integration of I_{Kr}-blockades has been described in **Appendix 1**. We used the forward Euler method for integral calculation.[8,9,15]

The transmural gradient (electrical heterogeneity through the ventricular wall) was achieved with the distribution through the epicardial, mid-myocardial (M-cell), and endocar-

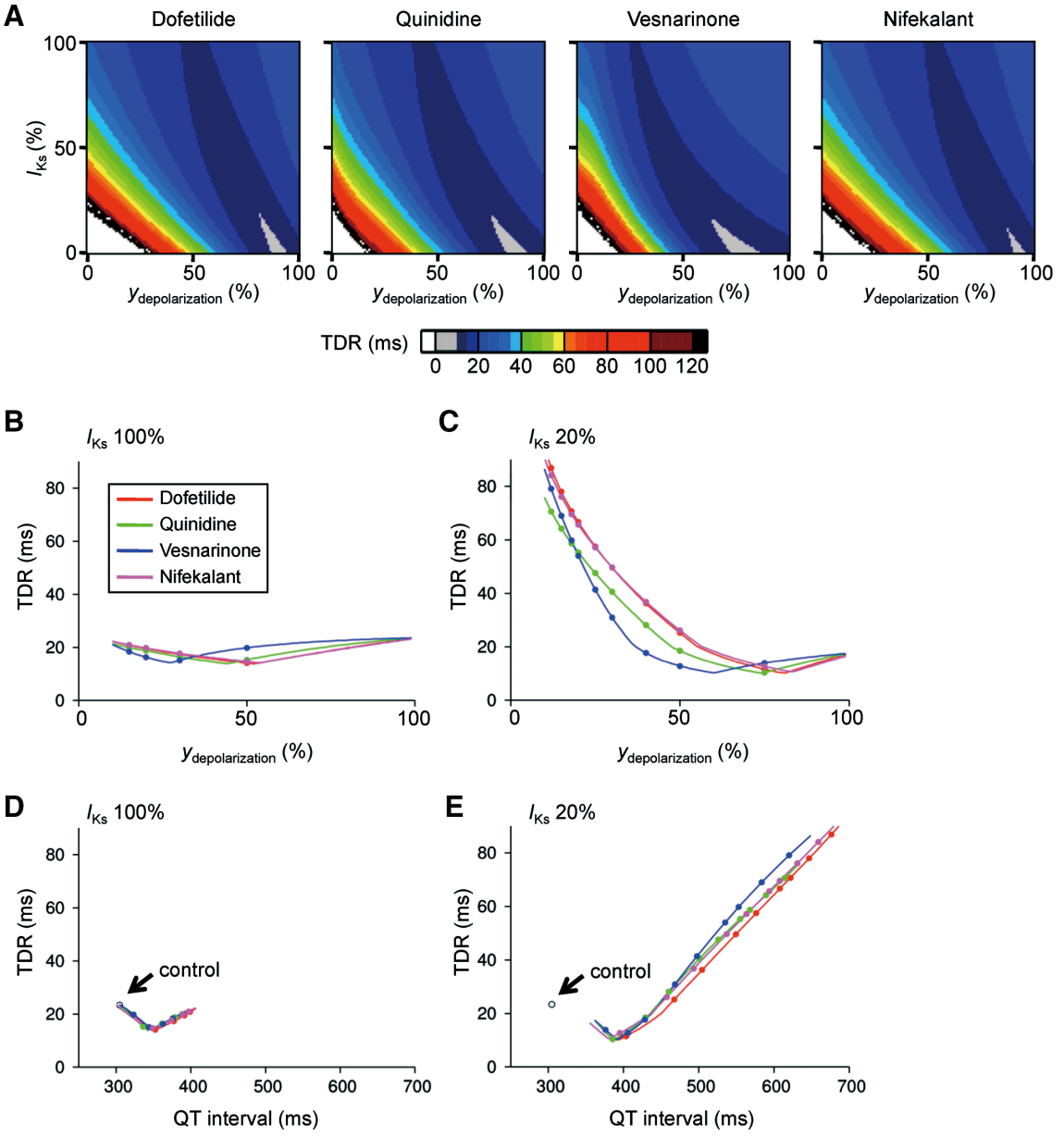

Figure 3. (**A**) Transmural dispersion of repolarization (TDR) 2-dimensional (D) maps in the presence of each drug (pacing cycle is 1,000 ms) in the transmural 1-D model. White areas indicate conditions where TDR could not be calculated because the action potential duration was longer than the length of the pacing cycle. (**B**, **C**) TDR as a function of $y_{depolarization}$ in the presence of each drug in the original and reduced I_{Ks} models, respectively. (**D**, **E**) Relationship between TDR and QT interval in the original and the reduced I_{Ks} models, respectively.

dial layers (**Figures 1A** and **1B**) with thicknesses of 0.35 cm, 0.50 cm, and 0.15 cm, respectively. We configured the total thickness to be 1.0 cm by considering the human left ventricle. According to experimental data, the M-cell layer was located deep within the subendocardium.[5] These spatial settings can be found in our previous publication,[16] which demonstrated that the normal 12-lead electrocardiograms were properly reconstructed under those spatial settings. Electrical settings were achieved by modifications of I_{Kr}, I_{Ks}, I_{to}, and I_{Kp}.[13] **Figures 1C** and **1D** show the control for the transmural gradient used in this study.

The ventricular wall slab model was 6.0×6.0×1.0 cm, and consisted of 10,560,000 discrete myocardial units (**Figure 1A**). We considered a sufficiently large size that allows scroll waves to rotate during a simulation time. As a result, we used the same size as the ventricular wall slab model in our previous publication.[17] The tissue border was set to no-flux Neumann boundary conditions. The conduction velocity was set at 59, 18, and 40 cm/s in the *x*-, *y*-, and *z*-axes, respectively, based on experimental data.[5,18,19]

The TDR was quantified during transmural conduction by performing simulations of consistent endocardial pacing

using the 1-D model shown in Figure 1B. Thirty-one pacing stimuli of 5-ms duration and 20-μA strength were applied to the endocardial units at a cycle length of 1,000 ms to achieve steady state. After the last pacing stimulus, we measured APD and conduction time in all myocardial units of the 1-D model. The APD was measured at –75 mV (close to APD_{90}), then both TDR and QT interval were calculated. To visualize the effects of the various ion channel blockers on TDR, we adopted a 2-D mapping method.[13] We repeated simulations systematically with various I_{Ks} channel conductance levels in increments of 1% and various $y_{depolarization}$ (I_{Kr} amplitude).[13]

Scroll waves were generated using a S1-S2 cross-field stimulation (Figure 2).[17] A premature stimulus (S2), as a part of the globular shape, was applied when the refractory tail (S1 tail) of the 6th planar wave had just passed through the center of the ventricular wall slab model.

Potassium channels play a key role in the development of TDR, and therefore we modified I_{Ks} and I_{Kr} conductances independently to produce various TDR. In the present study, the reduced I_{Ks} model was an 80% reduction in the I_{Ks} original value (100%)[13] (Table).

We set the simulation time to 1,500 ms after the S2 stimulus due to computer performance. Except for a few cases of very long QT interval (>550 ms), this simulation time was enough for the scroll waves to rotate ≥6 times, which was generally considered as sustained tachyarrhythmia.[20] In addition, even in the cases of very long QT intervals, we considered the simulation time was enough to define sustained tachyarrhythmia because of the frequent wave breakups, which can increase the number of scroll waves during the simulation time.

Our preliminary simulations with significantly longer TDR and QT interval showed that frequent scroll wave breakups occurred immediately after the S2 stimulus. Thus, we strongly believe that the length of simulation time was sufficient to observe the scroll wave behavior in all of the simulations in this study.

The scroll wave filaments were expressed as a continuum of phase singularities, defined as spatial points where all phase values converged in a phase map.[21,22]

Results

Variations in TDR With I_{Kr}- and I_{Ks}- Blockade in a 1-D Transmural Model

Figure 3A shows the TDR as a function of I_{Ks} and $y_{depolarization}$, where $y_{depolarization}$ describes the degree of I_{Kr} blockade by dofetilide, quinidine, vesnarinone, and nifekalant at a pacing cycle of 1,000 ms in the transmural 1-D model (Figure 1B). At the I_{Ks} original value (I_{Ks} 100%) the TDR remained at ~20 ms, regardless of the $y_{depolarization}$ value (Figure 3B). The effect on the TDR was similar for all 4 I_{Kr}-blockers. In contrast, when the I_{Ks} was reduced to 20%, an inverse correlation was observed between the TDR and the $y_{depolarization}$ (Figure 3C). Under these conditions, dofetilide and nifekalant produced significantly longer TDR values than did quinidine or vesnarinone.

As shown in Figure 3D, the simulated ECG with various $y_{depolarization}$ values revealed neither a marked prolongation of TDR nor a long QT interval at I_{Ks} 100%, and we observed a dip in TDR with a QT interval in the range below 400 ms. Similarly, we observed a dip in TDR as well in I_{Ks} 20% case; however, we found marked prolongation of TDR with a positive correlation with a QT interval (Figure 3E).

The effect of the 4 I_{Kr}-blockers on the relationship between the TDR and QT interval was quite similar at I_{Ks} 100% (Figure 3D). In contrast, at I_{Ks} 20%, the 4 I_{Kr}-blockers produced different effects on the relationship between the TDR and QT interval. For example, when the QT interval was above ~500 ms, vesnarinone and dofetilide produced the longest and shortest TDR, respectively. Thus, a reduction in I_{Ks} facilitated the I_{Kr} blockade-mediated increase in TDR and revealed the differential effects of the I_{Kr}-blockers on the TDR (Figures 3C and 3E).

TDR Influence on Filament Dynamics in the Ventricular Wall

The TDR was 23.7 ms in the control condition ($y_{depolarization}$ 100% and I_{Ks} 100%; Figure 4A, Leftmost panel). With this TDR, the mother-daughter type scroll wave re-entries were sustained for 1,500 ms after S2 onset (Figure 4A, Middle 3 panels; Supplementary Movie 1). The mother re-entry rotated around a transmural I-shaped filament that bent spontaneously and occasionally fragmented. The fragmented filaments were classified into 2 types: the S-filament (blue) in which both fragment ends touched the epicardial or endocardial surface, and the NS-filament (green) in which the fragment ends did not touch a surface. The S-filament accompanied the rotating scroll wave and the NS-filament signified the wavebreak of the drifting (non-rotating) scroll wave. Thus, the daughter scroll wave re-entries were always accompanied by the fragmented S-filaments generated by the occasional fragmentations of the bent I-shaped filament of the mother scroll wave re-entry.

The total length of the S-filaments (blue line) and NS-filaments (green line) varied markedly with time (Figure 4A, Rightmost panel). Both the filament bending and the filament fragmentations increased the total length of the S-filaments. Filaments that were aligned parallel to the myocardial fiber transformed from S-filaments into NS-filaments (corresponding to a decrease in the S-filaments length and an increase in the NS-filament length). A filament shift resulting in a collision between the NS-filament and the tissue boundaries (lateral edges of the ventricular wall slab) caused a decrease in the total length of the NS-filaments. The filaments aligned on the border between the epicardial and mid-myocardial layers. The S-filament bent at the border between the epicardial and mid-myocardial layers, and the NS-filament aligned on the same border. The border between the epicardial and mid-myocardial layers was close to the plane with the maximum slope of transmural gradient in repolarization time.

The smaller 19.5 ms TDR (Figure 4B, Leftmost panel) produced by the dofetilide-type I_{Kr} blockade and original I_{Ks} ($y_{depolarization}$ 20% and I_{Ks} 100%, respectively) resulted in the continuation of the S-filament associated with the single scroll wave re-entry and a short-lived NS-filament (Figure 4B, Middle 3 panels; Supplementary Movie 2). In this example, the scroll wave re-entry was terminated by the annihilation of all S-filaments at 1,475 ms after the S2 onset.

When the bending and fragmentation of the S-filaments were restrained, the total length of both the S- and NS-filaments was shorter, compared with the control condition (Figures 4A and 4B, Rightmost panels). The short-lived NS-filaments aligned parallel to the myocardial fibers and were located in the mid-myocardial layer in the vicinity of the epicardium.

The larger 78.0 ms TDR (Figure 4C, Leftmost panel) produced by the dofetilide-type I_{Kr} blockade and reduced I_{Ks} ($y_{depolarization}$ 15% and I_{Ks} 20%) resulted in frequent scroll wave breakups accompanied by the fragmentation and/or neogenesis of the S-filaments (Figure 4C, Middle 3 panels;

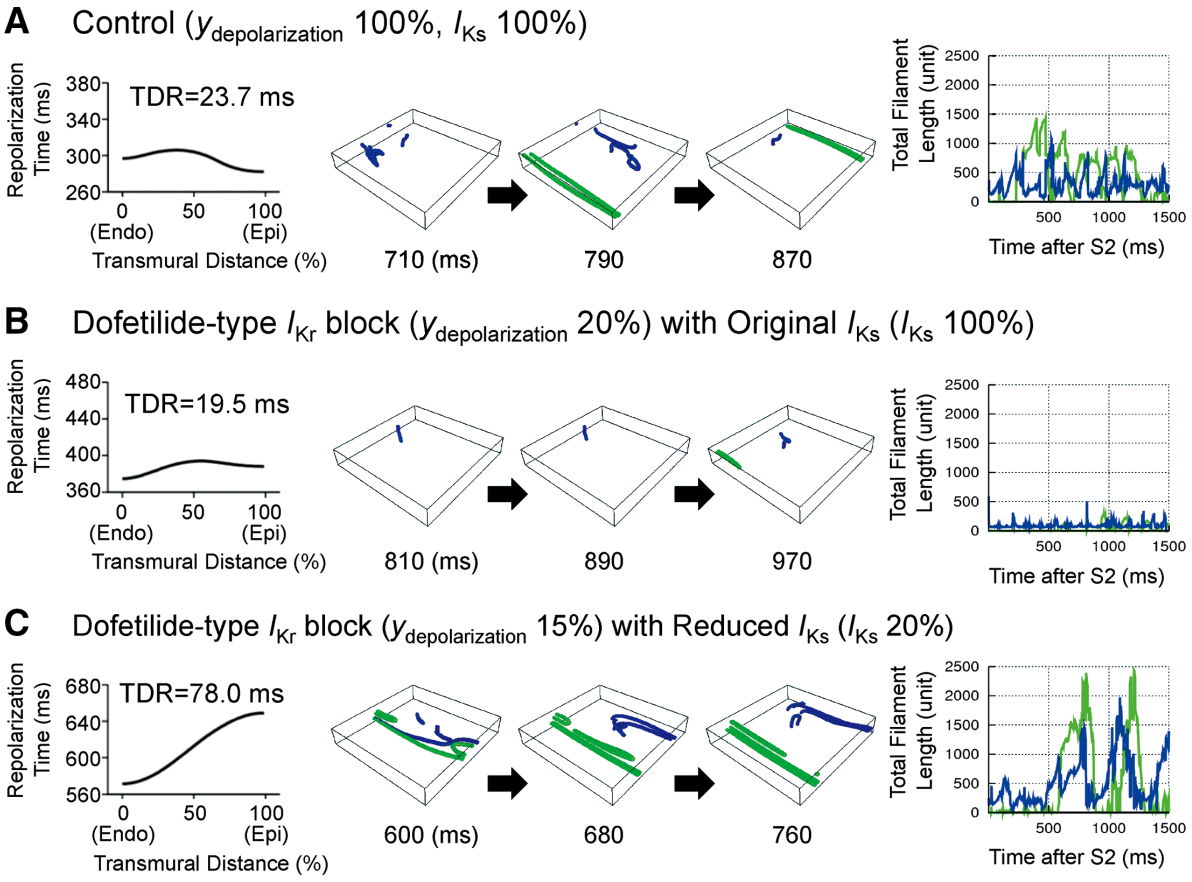

Figure 4. The transmural distribution of repolarization time (**Leftmost panel**), the snapshots of filament dynamics (**Middle 3 panels**), and the temporal variation of the total filament length in the ventricular wall slab model (**Rightmost panel**). S-filament (blue) and NS-filament (green) lengths. Repolarization time (*y*-axis in leftmost panel) equals APD_{90} plus conduction time in each myocardial unit. Transmural distances at 0% and 100% represent epicardium and endocardium, respectively. Supplemental online data I through III are movie supplements corresponding to panels (**A**) through (**C**), respectively. APD, action potential duration; TDR, transmural dispersion of repolarization

Supplementary Movie 3). The fragmentation of the I-shaped S-filament was derived from the filament bending. In contrast, the neogenesis of the U-shaped S-filament was derived from the wavefront-wavetail interaction. Most of the NS-filaments were derived from the S-filaments that were aligned parallel to the myocardial fibers located at the mid-myocardial layer in the vicinity of the endocardium. The alignment location was in the vicinity of the plane with the maximum slope of transmural gradient in repolarization time, whereas the alignment location was shifted toward the plane with the shorter repolarization time. Under these conditions, the total length of the S- and NS-filaments varied markedly with time, similar to the control condition; however, the total filament lengths were much longer than the control condition (**Figures 4A** and **4C**, **Rightmost panels**). The filament neogenesis resulting from the wavefront-wavetail interaction was responsible for an increase in the total length of S-filaments. The other behaviors of the filaments were similar to those in the control condition (see **Supplementary Movies 1** and **3**).

Relationship Between TDR and Total S-Filament Length

Simulations of scroll wave re-entries were conducted in the same ventricular wall slab model using the 4 I_{Kr}-blockers in various $y_{depolarization}$ and I_{Ks} conditions: original I_{Ks} (I_{Ks} 100%) with a $y_{depolarization}$ of 50%, 30%, 20%, and 15% (filled circles in **Figures 3B** and **3D**) and reduced I_{Ks} (I_{Ks} 20%) with $y_{depolarization}$ of 75%, 50%, 40%, 30%, 25%, 20%, 18%, 15%, and 12% (filled circles in **Figures 3C** and **3E**). The relationship between the TDR and the average total S-filament length during the simulation time (1,000 ms from 500 ms after the S2 stimulus) is shown in **Figure 5**.

The TDR was 23.7 ms in the control condition and the average S-filament total length was 311.5 units (refer to a black filled circle with an arrow in **Figure 5**).

When the I_{Kr}-blockade produced a TDR ranging from 23.7 to 58.3 ms, the average S-filament total length was significantly shorter than that observed in the control condition (~150 units). The filament dynamics (not shown) were similar to those shown in **Figure 4B**; both the bending and fragmentation of the S-filaments were restrained, and, as a consequence, the transmural I-shaped S-filaments were sustained and the NS-filaments were short-lived.

When the I_{Kr}-blockade produced a TDR shorter than 23.7 ms, the average S-filament total length was increased by the decrease in the TDR, and reached ~330 units, approximately the same length observed in the control condition.

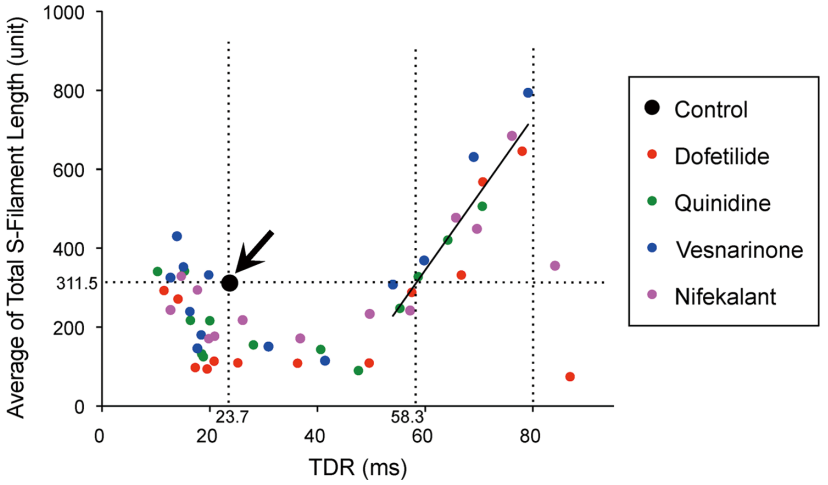

Figure 5. Relationship between the transmural dispersion of repolarization (TDR) and the average S-filament total length.

The filament dynamics (not shown) were similar to those shown in Figure 4A; the bending and fragmentation of the S-filaments and the transition from S-filaments to NS-filaments occurred frequently.

When the TDR ranged from 58.3 to 80.0 ms, the average S-filament total length increased in proportion to the increase in TDR, and the length was ~800 units when the TDR reached ~80 ms. The filament dynamics (not shown) were similar to those shown in Figure 4C; bending, fragmentation, and neogenesis of the S-filaments were frequently observed, and the transition from S-filaments to NS-filaments occurred more often.

When the TDR was longer than 80 ms, the average S-filament total length was short, because the scroll wave re-entries spontaneously terminated and the accompanying filaments were short-lived (not shown).

Thus, the I_{Kr}-blockers, dofetilide, quinidine, vesnarinone, and nifekalant, did not change the relationship between the TDR and the average S-filament total length (Figure 5), but they did have different effects on TDR duration (Figures 3C and 3E).

Discussion

The present study examined the role of TDR in sustained scroll wave re-entry, and provided a novel analysis of the mechanisms underlying sustained tachyarrhythmias. We analyzed the filament dynamics to simplify and quantify the complex spatiotemporal activity during scroll wave re-entry. The major findings of the present study are:

(1) Reduced I_{Ks} enhanced the I_{Kr} block-mediated increase in the TDR.

(2) A mild increase in the TDR restrained the scroll wave breakup and shortened the total filament length, whereas a marked increase in the TDR facilitated the scroll wave breakup and increased the total filament length.

The Role of TDR in the Induction of Arrhythmia

The balance of initiation, termination, and breakup of the scroll waves determines the sustainment of ventricular tachyarrhythmias. The present study analyzed scroll wave behavior in response to various TDR, with the aim of clarifying the relationship between the TDR and the maintenance of ventricular tachyarrhythmias.

It is widely accepted that the TDR or electrophysiological heterogeneity at the tissue level induces re-entrant arrhythmias. Noda et al suggested in a clinical study that TdP might occur as a result of enlarged TDR, leading to the first re-entrant excitation in patients with congenital LQTS.[23] El-Sherif et al[24] showed that TDR was linked to the genesis of TdP in the canine LQTS model, and Kozhevnikov et al[25] demonstrated that dofetilide significantly increased TDR which, in turn, increased vulnerability to hypertrophic heart. Furthermore, Akar et al showed that the regional distribution of M-cells underlies the re-entrant mechanism of TdP in the canine LQTS model.[2]

T-wave alternans is known as a predictor of arrhythmic events[26,27] and discordant T-wave alternans is associated with a greater propensity to develop ventricular tachyarrhythmias.[28] Chinushi et al showed that the discordant T-wave alternans derived from both the heterogeneous distribution of the diastolic interval and the regional differences in the restitution properties.[29] The majority of clinical and experimental studies have suggested that arrhythmogenesis is primarily caused by a large degree of electrophysiological heterogeneity or TDR that activates the TdP/VF mechanism. Similarly, in the 2-D simulations, Clayton and Holden reported a close relationship between the increase in APD dispersion and the initiation of re-entrant arrhythmias.[30]

In contrast, findings reported by our colleagues numerically indicated that TDR is a predictor of drug-induced TdP, independent of APD prolongation.[13] They suggested that although early afterdepolarization, resulting from QT prolongation, plays an important role in triggering repetitive activation, an increase in TDR might be an independent substrate for re-entry initiation, an underlying mechanism for the perpetuation of ventricular tachyarrhythmias.[13] However, in their study,[13] the epicardial, mid-myocardial, and endocardial cell models[13] were not assembled into a 3-D ventricular wall with cell-to-cell coupling. Thus, in the present study, we extended the cellular level simulations into the 3-D tissue level. Our model included appropriate cell-to-cell coupling, wall thickness, and a transmural repolarization gradient. In the 3-D ventricular wall slab model, we found that the slight increase in TDR evoked by mild I_{Kr} blockade was antiarrhythmic, because it restrained scroll wave breakup, whereas the marked increase in TDR evoked by moderate I_{Kr} blockade was proarrhythmic because it facilitated scroll wave breakup.

This finding suggested that the induction of a tachyarrhythmia could be separated into initiation and maintenance stages, and the maintenance stage should be investigated in a 3-D model of the myocardium.

The Degree of TDR Determines Filament Dynamics

Filament dynamics are directly related to scroll wave behavior. Clayton and Holden revealed the details of filament dynamics during VF (eg, changes in the number of filaments, genealogical tree, distributions in length, and lifetime) in an anatomically-detailed simulation of canine ventricles.[31]

Our investigation of the relationship between TDR and QT interval did not reveal a one-to-one relationship (**Figure 3E**). It is widely accepted that the long QT interval with a sufficiently steep APD restitution curve increases the wavefront-wavetail interaction, resulting in scroll wave breakups. In contrast, as shown in **Figure 4** and the related supplementary movies, the filament bending was caused by the difference in APD among the endocardial, mid-myocardial, and epicardial layers (ie, TDR) rather than the longest APD among the 3 layers (ie, QT interval). Therefore, we believe that the TDR is an independent determining factor of scroll wave filament dynamics. Furthermore, our findings suggest that the total length of the S-filament depends on the degree of the TDR, and that a large TDR facilitates the sustainment of re-entrant ventricular tachyarrhythmias.

I_{Ks} Reduction Facilitates the I_{Kr} Block-Mediated TDR Increase

We found that different types of I_{Kr}-blockers changed TDR only when the I_{Ks} was reduced (**Figures 3C** and **3E**). This finding is similar to that reported by our colleagues in a cellular level simulation study.[13] I_{Ks} suppression corresponds to mimicking of a KCNQ1 defect, called LQT1. Additionally, latent LQTS and increasing TDR appear under I_{Ks} suppression. Burashnikov et al demonstrated that a prominent I_{Ks} was responsible for the resistance to the arrhythmogenic effects of I_{Kr} blockade in the canine heart.[32] I_{Ks} reduction in our simulations is within the range of LQT1 patients[33] and our simulations are consistent with their data.[32]

Longer TDR Increase the Critical Mass of the Myocardium

When TDR was longer than 80.0 ms, the average S-filament total length was shorter than it was at the control value (**Figure 5**). This might be explained by an increase in the critical mass of the myocardium as a result of the extended scroll wavelength[34,35] required to sustain TdP/VF. Scroll wave re-entry cannot continue to rotate spontaneously in an insufficient amount of myocardial tissue. The critical mass is then defined as the amount of myocardial mass that is incapable of maintaining the self-rotated scroll wave.[34,35] Our preliminary simulations revealed that at a TDR of 105.6 ms, the critical mass of the myocardium for a scroll wave re-entry was 9.0×9.0×1.0 cm, which was larger than that used in our study.

Physiological and Clinical Implications

The TDR has traditionally been thought to initiate rather than sustain ventricular tachyarrhythmias, and the roles of the QT interval and the TDR in the ventricular tachyarrhythmia have been ambiguous. In contrast, the present study clearly demonstrated that the TDR played a key role in the sustainment of ventricular tachyarrhythmias, based on scroll wave re-entries. We have shown that with a TDR longer than 58.3 ms, scroll wave breakup, which is important for the maintenance of ventricular tachyarrhythmias, is the result of both the fragmentation by filament bending and filament neogenesis by the wavefront-wavetail interaction. However, wavefront-wavetail interaction was hardly observed with a TDR shorter than 58.3 ms. Thus, we suggest that whereas the long QT interval might increase the wavefront-wavetail interaction, a large TDR can facilitate bending and fragmentation of filaments, causing scroll wave breakups.

In hypertrophied cardiac myocytes, normal transmural distribution of membrane current density has been reported to be decreased, resulting in T-wave inversion.[36,37] However, hypertrophied cardiomyocytes are susceptible to ventricular tachyarrhythmias. TDR should be within certain range, and both very small and very large TDR might be arrhythmogenic.

Our simulation results suggest that avoiding both a long QT interval and a large TDR is necessary to restrain inherent or drug-induced ventricular tachyarrhythmias at both the initiation stage and the maintenance stage leading up to tachyarrhythmias. Additionally, our simulation results suggest that the M-cell layer restrains degeneration of ventricular tachyarrhythmias by facilitating the transition from the S-filaments of scroll wave re-entries to the short-lived NS-filaments in the control condition.

Study Limitations

We did not consider rotational anisotropy because our principal goal was to investigate the role of the TDR in scroll wave behavior. From a structural point of view, we did not use rugged or curved tissue. Furthermore, we did not consider the anatomical features and topology (ie, septum, RV, and Purkinje fiber networks). In addition, a previous experimental study suggested a different distribution of M-cells within the ventricular wall.[2] The scroll wave behavior in such anatomically-based models might be far more complex than in the 3-D ventricular wall slab model employed in this study. Despite these limitations, we believe that our major findings are correct. Finally, as an action potential model, we employed the modified Luo-Rudy dynamic model rather than the human ventricular model. However, the modified Luo-Rudy dynamic model satisfied the conditions of transmural heterogeneity by producing a physiological TDR.

Conclusions

This study suggests that the degree of the TDR might determine the sustainment of ventricular tachyarrhythmias by controlling of the dynamics of the filaments accompanying scroll wave re-entries, and therefore provides mechanistic insight into the role of the TDR in ventricular arrhythmogenesis.

Acknowledgments

This work was supported by Grant-in-Aid for Scientific Research (C) 21500420, (C) 21590909, Young Scientists (B) 21790717, Innovative Areas (22136011) and the Global COE Program from Ministry of Education, Culture, Sports, Science and Technology of Japan.

References

1. Roden DM. Drug-induced prolongation of the QT interval. *N Engl J Med* 2004; **350:** 1013–1022.
2. Akar FG, Yan GX, Antzelevitch C, Rosenbaum DS. Unique topographical distribution of M cells underlies reentrant nechanism of Torsade de Pointes in the long-QT syndrome. *Circulation* 2002; **105:** 1247–1253.
3. Akar FG, Rosenbaum DS. Transmural electrophysiological heterogeneities underlying arrhythmogenesis in heart failure. *Circ Res* 2003; **93:** 638–645.
4. Shimizu W, Antzelevitch C. Sodium channel block with mexiletine

is effective in reducing dispersion of repolarization and preventing torsade de pointes in LQT2 and LQT3. *Circulation* 1997; **96:** 2038–2047.
5. Yan GX, Shimizu W, Antzelevitch C. Characteristics and distribution of M cells in arterially perfused canine left ventricular wedge preparations. *Circulation* 1998; **98:** 1921–1927.
6. Belardinelli L, Antzelevitch C, Vos MA. Assessing predictors of drug-induced torsade de pointes. *Trends Pharmacol Sci* 2003; **24:** 619–625.
7. Diego JMD, Belardinelli L, Antzelevitch C. Cisapride-induced transural dispersion of repolarization and torsade de pointes in the canine left ventricular wedge preparation during epicardial stimulation. *Circulation* 2003; **108:** 1027–1033.
8. Ashihara T, Suzuki T, Namba T, Inagaki M, Ikeda T, Ito M, et al. Simulated electrocardiogram of spiral wave reentry in a mathematical ventricular model. *In*: Yamaguchi T, editor. Clinical application of computational mechanics to the cardiovascular system. Tokyo: Springer-Verlag, 2000; 205–216.
9. Nakazawa K, Suzuki T, Ashihara T, Inagaki M, Namba T, Ikeda T, et al. Computational analysis and visualization of spiral wave reentry in a virtual heart model. *In*: Yamaguchi T, editor. Clinical application of computational mechanics to the cardiovascular system. Tokyo: Springer-Verlag, 2000; 217–241.
10. Winfree AT. Electrical turbulence in three-dimensional heart muscle. *Science* 1994; **266:** 1003–1006.
11. Faber GM, Rudy Y. Action potential and contractility changes in $[Na^+]_i$ overloaded cardaic myocytes: A simulation study. *Biophys J* 2000; **78:** 2392–2404.
12. Findlay I, Suzuki S, Murakami S, Kurachi Y. Physiological modulation of voltage-dependent inactivation in the cardiac muscle L-type calcium channel: A modeling study. *Prog Biophys Mol Biol* 2008; **96:** 482–498.
13. Suzuki S, Murakami S, Tsujimae K, Findlay I, Kurachi Y. In silico risk assessment for drug-induction of cardiac arrhythmia. *Prog in Biophys Mol Biol* 2008; **98:** 52–60.
14. Hosaka Y, Iwata M, Kamiya N, Yamada M, Kinoshita K, Fukunishi Y, et al. Mutational analysis of block and facilitation of HERG current by a class III anti-arrhythmic agent, nifekalant. *Channels* 2007; **1:** 198–208.
15. Suzuki T, Ashihara T, Inagaki M, Namba T, Ikeda T, Nakazawa K. A high-performance computation method for simulation of cardiac excitation propagation using a supercomputer. *In*: Yamaguchi T, editor. Clinical application of computational mechanics to the cardiovascular system. Tokyo: Springer-Verlag, 2000; 193–204.
16. Suzuki T, Inagaki M, Toda T, Yao T, Namba T, Suzuki R, et al. How M cell affects to the polarity of T waves: A computer simulation of the transmural distribution of APD in the ventricle wall. *IEICE Tech Rep* 2001; **101:** 21–28.
17. Ashihara T, Namba T, Ikeda T, Ito M, Kinoshita M, Nakazawa K. Breakthrough waves during ventricular fibrillation depend on the degree of rotational anisotropy and the boundary conditions: A simulation study. *J Cardiovasc Electrophysiol* 2001; **12:** 312–322.
18. Kadish A, Shinnar M, Moore EN, Levine JH, Balke CW, Spear JF. Interaction of fiber orientation and direction of impulse propagation with anatomic barriers in anisotropic canine myocardium. *Circulation* 1988; **78:** 1478–1494.
19. Saffitz JE, Yamada KA. Gap junction distribution in the heart. *In*: Zipes DP, Jalife J, editors. Cardiac electrophysiology: From cell to bedside, 3rd edn. Philadelphia: WB Saunders, 2000; 179–187.
20. Rodríguez B, Li L, Eason JC, Efimov IR, Trayanova NA. Differences between left and right ventricular chamber geometry affect cardiac vulnerability to electric shocks. *Circ Res* 2005; **97:** 168–175.
21. Larson C, Dragnev L, Trayanova N. Analysis of electrically induced reentrant circuits in a sheet of myocardium. *Ann Biomed Eng* 2003; **31:** 768–780.
22. Iyer AN, Gray RA. An experimentalist's approach to accurate localization of phase singularities during reentry. *Ann Biomed Eng* 2001; **29:** 47–59.
23. Noda T, Shimizu W, Satomi K, Suyama K, Kurita T, Aihara N, et al. Classification and mechanism of torsade de pointes initiation in patients with congenital long QT syndrome. *Euro Heart J* 2004; **25:** 2149–2154.
24. El-Sherif N, Caref EB, Yin H, Restivo M. The electrophysiological mechanism of ventricular arrhythmias in the long QT syndrome: Tridimensional mapping of activation and recovery patterns. *Circ Res* 1996; **79:** 474–492.
25. Kozhevnikov DO, Yamamoto K, Robotis D, Restivo M, El-Sherif N. Electrophysiological mechanism of enhanced susceptibility of hypertrophied heart to aquired torsade de pointes arrhythmias. *Circulation* 2002; **105:** 1128–1134.
26. Kim JW, Pak HN, Park JH, Nam GB, Kim SK, Lee HS, et al. Defibillator electrogram T wave alternans as a predictor of spontaneous ventricular tachyarrhythmias in defibrillator recipients. *Circ J* 2009; **73:** 55–62.
27. Maeda S, Nishizaki M, Yamawake N, Ashikaga T, Shimada H, Asano M, et al. Ambulatory ECG-based T-wave alternans and heart rate turbulence predict high risk of arrhythmic events in patients with old myocardial infarction. *Circ J* 2009; **73:** 2223–2228.
28. Chinushi M, Restivo M, Caref EB, El-Sherif N. Electrophysiological basis of arrhythmogenecity of QT/T alternans in the long-QT syndrome: Tridimensional analysis of the kinetics of cardiac repolarization. *Circ Res* 1998; **83:** 614–628.
29. Chinushi M, Kozhevnikov D, Caref EB, Restivo M, El-Sherif N. Mechanism of discordant T wave alternans in the in vivo heart. *J Cardiovasc Electrophysiol* 2003; **14:** 632–638.
30. Clayton RH, Holden AV. Dispersion of cardiac action potential duration and the initiation of re-entry: A computational study. *Biomed Eng Online* 2005; **4:** 11.
31. Clayton RH, Holden AV. Filament behavior in a computational model of ventricular fibrillation in the canine heart. *IEEE Trans Biomed Eng* 2004; **51:** 28–34.
32. Burashnikov A, Antzelevitch C. Prominent I_{Ks} in epicardium and endocardium contributes to development of transmural dispersion of repolarization but protects against development of early afterdepolarizations. *J Cardiovasc Electrophysiol* 2002; **13:** 172–177.
33. Viswanathan PC, Rudy Y. Pause induced early afterdepolarizations in the long QT syndrome: A simulation study. *Circ Res* 1999; **42:** 530–542.
34. Zipes DP, Fischer J, King RM, Nicoll AD, Jolly WW. Termination of ventricular fibrillation in dogs by depolarizing a critical amount of myocardium. *Am J Cardiol* 1975; **36:** 37–44.
35. Kim YH, Garfinkel A, Ikeda T, Wu TJ, Athill CA, Weiss NW, et al. Spatioteporal complexity of ventricular fibrillation revealed by tissue mass reduction in isolated swine right ventricle. *J Clin Invest* 1997; **100:** 2486–2500.
36. Bryant SM, Shipsey SJ, Hart G. Normal regional distribution of membrane current density in rat left ventricle is altered in catecholamine-induced hypertrophy. *Cardiovasc Res* 1999; **42:** 391–401.
37. Rozanski GJ, Xu Z, Zhang K, Patel KP. Altered K^+ current of ventricular myocytes in rats with chronic myocardial infarction. *Am J Physiol Heart Circ Physiol* 1998; **274:** 259–265.

Appendix 1

Integration of 4 Representative Types of I_{Kr}-Blockade

To integrate 4 representative types of I_{Kr}-blockade, we modified I_{Kr} currents as follows:[13]

$$I_{Kr} = y \cdot \overline{G}_{Kr} \cdot X_r \cdot R \cdot (V - E_{Kr}),$$

where y is the fraction of I_{Kr} that is not blocked, $\overline{G}_{Kr}$ is the maximum conductance of I_{Kr}, X_r is the time-dependent activation gate, R is the time-independent inactivation gate, V is the membrane potential, and E_{Kr} is the reversal potential.

$y_{depolarization}$ represents I_{Kr} amplitude.[13] The dofetilide-induced blockade is voltage- and time-independent and the y is constant and is equal to $y_{depolarization}$.[13]

The quinidine-induced blockade is fast-voltage- and time-dependent. The y is calculated by the following first order differential equation:[13]

$$\frac{dy}{dt} = \frac{(y_\infty - y)}{\tau},$$

where y_∞ is the steady-state value of the fraction of I_{Kr} that is not blocked by quinidine-type drug, and τ is the time-constant for y.

The unbinding rate constant (α) and the binding rate constant (β) are obtained from experimental data.[13] The steady-state value of y (y_∞) and the time-constant for y (τ) are expressed as follows:

$$y_\infty = \frac{\alpha}{\alpha + \beta},$$

$$\tau = \frac{1}{\alpha + \beta},$$

$$\alpha = 0.5716 + 0.7522 \cdot \exp(0.05094 \cdot V)$$

$$\beta = 0.7522 \cdot \exp(0.05094 \cdot V)\left(\frac{1}{y_{depolarization}} - 1\right),$$

where $y_{depolarization}$ is the limit set for the minimum of unblocked I_{Kr} in the presence of quinidine.

The vesnarinone-induced blockade is slow-voltage- and time-dependent as follows:[13]

$$\alpha = 0.5$$

$$\beta = \frac{0.5 \cdot \left(\frac{1}{y_{depolarization}} - 1 \right)}{1 + \exp\left(\frac{-(V+16.5)}{12.6} \right)}.$$

The nifekalant-induced blockade is voltage- and time-independent, and is similar to dofetilide-induced blockade. The y is constant and is equal to $y_{depolarization}$. The nifekalant-induced blockade was simulated using a steady-state activation curve of I_{Kr} kinetics shifted positively 20 mV, as reported by Hosaka et al:[14]

$$X_{r\infty} = 1/\{1+\exp[-(V+41.5)/7.5]\},$$

where $X_{r\infty}$ is the steady-state value of the I_{Kr} activation gate.

Appendix 2

Methods to Measure TDR, QT Interval, and Filament Length

We defined the depolarization time in each myocardial unit as the time when the membrane potential go above –75 mV, and the repolarization time as the time when the membrane potential go below –75 mV. Then, the APD was defined as the interval between the depolarization time and the repolarization time in each myocardial unit. Further, the TDR was defined as the interval between the earliest repolarization and the last repolarization in the 1-D model,[13] and the QT interval was defined as the interval between the earliest depolarization and the last repolarization (refer **Figure 1D**).[13]

The scroll wave filaments were expressed as a continuum of phase singularities, defined as spatial points where all phase values converged in a phase map.[21,22] We counted the number of units detected as the filament locations and considered the number as a filament length.

Supplementary files

Movie 1. The scroll wave behavior and filament dynamics corresponding to **Figure 4A**.

Movie 2. The scroll wave behavior and filament dynamics corresponding to **Figure 4B**.

Movie 3. The scroll wave behavior and filament dynamics corresponding to **Figure 4C**.

Please find supplementary file(s);
http://dx.doi.org/10.1253/circj.CJ-10-0071